

Learning Dense UV Completion for Human Mesh Recovery

Yanjun Wang¹ Qingping Sun² Wenjia Wang³ Jun Ling¹
 Zhongang Cai² Rong Xie¹ Li Song^{1,†}

¹ Shanghai Jiao Tong University ² SenseTime Research ³ Shanghai AI Laboratory

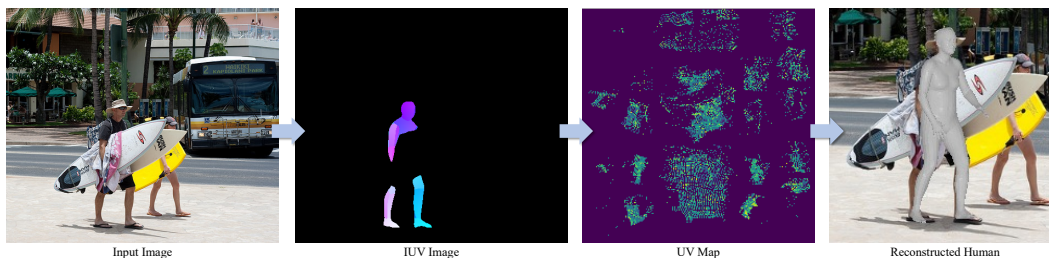


Figure 1: Our method consists of two key steps: 1) estimates the dense UV map of the obscured body and mask out the occlusion regions; 2) performs UV-based feature wrapping and completion for future mesh reconstruction.

Abstract

Human mesh reconstruction from a single image is challenging in the presence of occlusion, which can be caused by self, objects, or other humans. Existing methods either fail to separate human features accurately or lack proper supervision for feature completion. In this paper, we propose Dense Inpainting Human Mesh Recovery (DIMR), a two-stage method that leverages dense correspondence maps to handle occlusion. Our method utilizes a dense correspondence map to separate visible human features and completes human features on a structured UV map dense human with an attention-based feature completion module. We also design a feature inpainting training procedure that guides the network to learn from unoccluded features. We evaluate our method on several datasets and demonstrate its superior performance under heavily occluded scenarios compared to other methods. Extensive experiments show that our method obviously outperforms prior SOTA methods on heavily occluded images and achieves comparable results on the standard benchmarks (3DPW).

1. Introduction

Reconstructing human mesh from a single image broadens a broad view of applications, such as human motion analysis, digital human animation, augmented reality, and

human-world interactions. However, occlusion is a long-standing obstacle that hinders the model’s performance for in-the-wild images. Occlusion can be divided into three categories: self-occlusion, the occlusion of certain parts caused by the body itself; object occlusion, the occlusion caused by other objects in the environment; inter-human occlusion, the occlusion caused by closely overlapped humans. Among them, self and object occlusion can all be seen as non-human occlusion, as they only lack information rather than have confusing information introduced by other humans.

The widespread parametric model SMPL [37, 44] has facilitated rapid progress in this field in recent years, with various approaches proposed to improve the model generalization performance. Most of them aim at completing the missing features caused by occlusion. HMR [23] proposes to use an adversarial prior to correct the implausible poses. This can be seen as a completion from the pose prior. But the distribution of the prior largely depends on its dataset. Thus, the variety of the poses is limited by the conclusiveness of the prior datasets. Other methods seek cues from the image feature. PARE [27] proposes a part-attention mechanism, which can utilize local features from visible body parts to complete the occluded body’s feature. But for these image-based methods, the completion method lacks intermediate supervision, and their performance is often limited.

Human occlusion presents a significant challenge compared to non-human occlusion because it provides ambiguous information that can lead to difficulties in distinguishing

*LS[†] is the corresponding author.

between different body parts, such as limbs and torso. In response to this challenge, several methods have been proposed to model multiple humans. ROMP [46] and BEV [47] are two representative multi-person methods that regress multiple persons directly. They represent humans with 2D or 3D heat maps and solve the position ambiguity of humans in various ways. However, due to limitations in resolution, these methods may not accurately regress every person, and they may not have solutions for occluded body parts. Two-stage methods designed to predict one person at a time tend to focus on separating and identifying the true human to predict. OCHMR [24] utilizes a ROMP-like center heat map. 3DCrowdNet[7] uses a keypoint heatmap. Pose2UV [18] combines segmentation with a keypoint heatmap for separation. But these heatmap or segmentation cues are only used as an auxiliary input and guide the network implicitly. These cues cannot clearly separate the predicted and occluded humans, which might introduce confusing features when two body parts are close enough.

In this work, we resort to solving general occlusion while maintaining relatively high performance. More specifically, a model takes as input a high-resolution image and has the ability to complete missing features with ground truth supervision. For the separation issue, we draw inspiration from the dense corresponding map, which regresses each pixel into a surface point on the human model. Previous studies [53, 52] prove that dense correspondence is beneficial for human reasoning. But their dense prediction is based on the image input, and weakly supervised, which means the prediction itself will be affected by occlusion. For the completion issue, OOH [57] utilizes a dense location map for direct supervision of the occluded vertices through inpainting. Compared to SMPL parameters, this approach provides much denser and more direct supervision. However, direct regression of vertices coordinates using this method requires more regulation to achieve a smooth surface.

Inspired by these methods utilizing dense correspondence, we propose Dense Inpainting Human Mesh Recovery (DIMR), a top-down, high-resolution method designed to solve different occlusions. To leverage the representative power of dense correspondence maps to separate human features, we utilize a dedicated network for dense correspondence map regression. The regressed dense map is much more accurate and sharp compared to an integrated module. Moreover, the network simultaneously performs human detection and dense map prediction, which is suited to the first stage of our module. But utilizing the dense map for parameter regression and occlusion handling is non-trivial. Given the UV nature of the dense map, we designed a feature-wrapping process to accurately separate human features and project them to a structured UV map. Based on this UV map, we further proposed an attention-based

mechanism to complete the occluded feature based on the other part’s features. And based on the attention, we derived part-wise human features to regress SMPL parameters. To further enhance the occlusion handling ability, we designed a feature inpainting training procedure that guides the network for feature completion with the unoccluded features. To validate our design, we conduct extensive experiments on the 3DOH [57], 3DPW [48], 3DPW-OC [48, 27] and 3DPW-PC [48] datasets. The results indicate that our model yields a higher accuracy under heavily occluded scenarios compared to other occlusion handling experiments and maintains a comparable accuracy on general human datasets.

In summary, our contributions are three folds:

- We introduce a novel way to utilize a dense correspondence map that learns human features reconstruction under heavy inter-person occlusion.
- We propose a mechanism utilizing visible features to complete occluded parts features to reason object occlusion. And designed a training mechanism with direct visible supervision to guide the completion.
- Our method achieves state-of-art results on occlusion datasets of 3DPW-PC, 3DPW-OC, and has a comparable accuracy on general datasets on 3DPW. Extensive experiments show that our method is capable of dealing with human mesh recovery under heavy occlusion.

2. Related Work

2.1. Human Mesh Recovery

Recovering 3D human pose and shape only from a single image is a challenging task due to the lack of multiview information and complicated human articulations. Most recent works can generally be divided into optimization-based methods and learning-based methods. Optimization-based methods [19, 31, 15, 3, 14] work by fitting a statistical human body model to the 2D cues extracted from the input image, such as 2D keypoints [3] or silhouette [31]. On the other hand, learning-based methods have gained significant traction in recent years and employ deep neural networks to estimate the 3D pose and shape of the human body, which can be further classified into two categories: model-based and model-free methods.

Model-based methods [23, 28, 27, 54, 46, 47, 32, 41, 8] leverage a deep neural network to regress the parameters of the human model. HMR [23] first utilizes CNN to extract the global features and then regresses the SMPL parameters. SPIN [29] combines the learning-based method (HMR) with the optimization-based method (SMPLify), which leads to accurate image-model alignment. CLIFF [33] proposes a new camera system to solve the inaccuracy of global

rotations under the cropped image. With a corrected camera system, it outperforms prior arts on a significant margin even with a simple HMR-like structure.

Leverage the efficiency of 3D mesh reconstruction tasks [10, 50, 51, 12, 55], model-free methods [30, 40, 6, 53, 34, 35, 5, 11] leverage a deep neural network to directly estimate the 3D coordinate of the human mesh. GraphCMR [30] is a milestone work, and it uses CNN to extract features from the input image at first and then uses GraphCNN [26] to estimate the 3D coordinates of the human mesh directly. Although GraphCNN considers local interactions among neighbor vertices, like HMR, GraphCMR only uses global features extracted from the image to recover the human mesh. Although the accuracy of unoccluded, single-person benchmarks have been increasing, these methods cannot generalize well to occlusion scenarios.

2.2. Occlusion-aware Human Mesh Recovery

Recent efforts that aim at solving occlusions mainly focus on two main groups: objects or human occlusions [47, 46, 57, 27, 7, 21]

For object occlusion, PARE [27] devises a part attention regressor to predict body-part-guided attention mask, which is helpful for the neural network to exploit information about the visibility of individual body parts to estimate occluded parts, but it overlooked the importance of global feature and the connection between different joints. OOH [57] proposes a method to complete the model from the surface prior. It maps the SMPL model to a UV image and masks out the pixel value of the occluded surface. It models occlusion completion as an image inpainting task, using the network to complete the occluded UV image value.

For inter-human occlusion, ROMP [46] proposes a collision-aware center heatmap to model multiple humans on the image. It builds a repulsive field of body centers that push away close body centers, making overlapping human body centers easier to distinguish. Jiang et al. [38] utilize an interpenetration loss to regular multiperson location based on instance segmentation. 3DCrowdNet [24] proposes to distinguish the target’s image feature with the occluded human with the guide of a 2D joint map. Compared to the sparse representation of a predicted human, our model utilizes a dense correspondence map to achieve accurate and dense image feature separation.

2.3. Dense Correspondence Learning

Dense human body representations [2, 53, 52] have been widely used in the analysis of humans. DecoMR [53] propose to estimate a dense correspondence map and wrapped the feature to UV space for coordinate regression. VisDB [52] predicts 3D heatmaps for human joints and vertices and the visibility for each vertex. These meth-

ods prove that dense correspondence is beneficial for human reasoning. But their dense prediction is based on the image input, and weakly supervised, which means the prediction itself will be affected by occlusion. DensePose [16] proposed a CNN-based system that regresses coordinates of the human body surface on the human image, which can be later utilized for feature transfer, human mesh regressing. This dedicated design has much higher accuracy and is capable of separating the features of occluded persons. Our model leverages its ability to predict accurate dense correspondence images.

3. Method

DIMR utilizes a human dense correspondence map, also called the IUUV image, to aggregate visible features of the occluded human as well as isolate the prediction subject from the overlapped human occlusion. This section begins with a brief overview of the SMPL [37] body model and subsequently discusses the design of our model. Based on the observation of current occlusion handling methods, we integrate the separation of human instances and the completion of human features with a dense IUUV image. To better separate human instances, we use the map to wrap the human feature to a specially designed UV map. Features are rearranged based on the body part they belong to. Given the structured UV feature. Also, we proposed an attention-based method to promote feature completion on the structured feature map. Finally, to better handle occlusion, we proposed a parallel training method to feed feature-level supervision to the network.

3.1. Preliminary

SMPL represents a 3D human mesh with $\mathcal{M}(\theta, \beta) \in \mathbb{R}^{6890 \times 3}$ where $\beta \in \mathbb{R}^{10}$ represents the first 10 coefficients for SMPL’s PCA surface shape, and $\theta \in \mathbb{R}^{24 \times 3}$ represents the joints rotations which include global rotations. Given the 3D mesh, the 3D joints can be calculated as $J_{3D} = \mathcal{J}\mathcal{M} \in \mathbb{R}^{J \times 3}$, $J = 24$ with a pretrained joint regressor \mathcal{J} .

We adopt a weak perspective camera system $\pi = (s, \mathbf{t})$, $\mathbf{t} \in \mathbb{R}^2$ to project the predicted body model to the image plane. Based on 3D joints and camera, we calculate the 2D joints following: $J_{2D} = s\Pi(\mathcal{J}\mathcal{M}) + \mathbf{t} \in \mathbb{R}^{J \times 3}$, where Π is orthographic projection.

Input Preparation. The pipeline of our model is shown in Figure 2. Given an uncropped image, we first utilize DensePose [16] to extract the IUUV map of every object. Based on each dense map and bounding box, our network takes the cropped image $I \in \mathbb{R}^{3 \times H \times W}$ and cropped IUUV image $M_{iuv} \in \mathbb{R}^{3 \times H \times W}$ as input. In M_{iuv} , the first channel $i \in \mathbb{R}^{H \times W}$ represents the segmentation of the human object, and the second and third channels are a two-

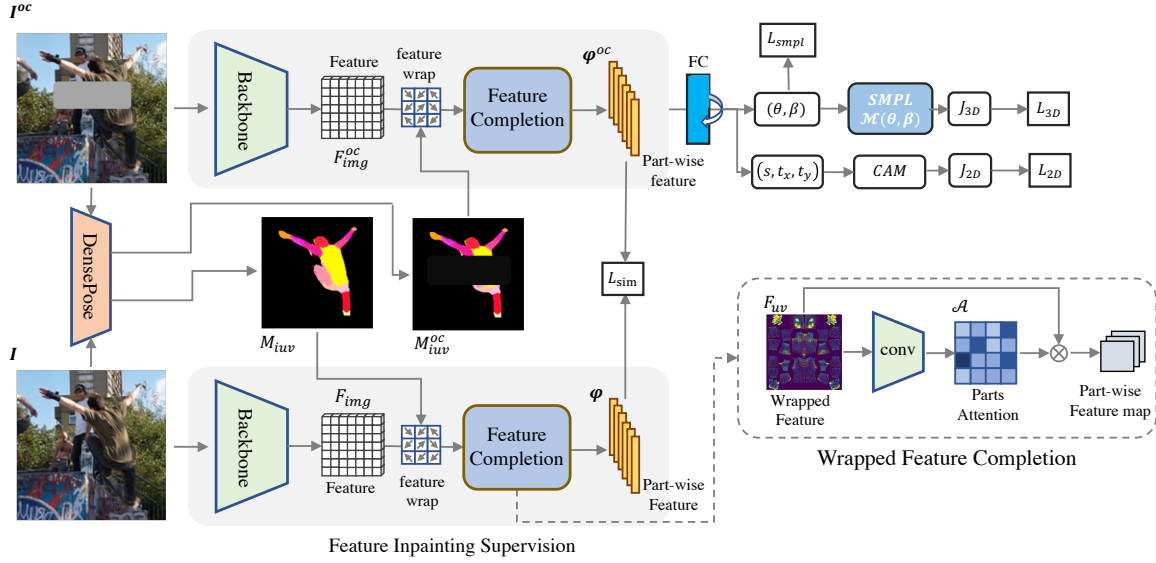


Figure 2: **Pipeline overview** Our model consists of a UV feature wrap module, a feature completion model, and an FC layer for SMPL parameter regression. Our network takes the image I and predicted IUV image M_{iuv} as input. The IUV image wraps the image feature to UV space. The attention-based feature completion module completes the occluded feature based on the visible ones. The inpainting training takes the original and occluded image as input, and uses the original feature as the supervision for the occluded feature.

dimensional coordinate $(u, v) \in \mathbb{R}^{2 \times H \times W}$, which represents the mapping location of this pixel on the UV map.

3.2. UV Based Feature Wrapping

We utilize an image encoder to encode the cropped image and obtain a feature map $F_{img} \in \mathbb{R}^{D \times H' \times W'}$. The feature wrapping module wraps the feature vector on F_{img} into a UV space feature map $F_{UV} \in \mathbb{R}^{D \times H' \times W'}$ according to the following equation:

$$F_{UV}(u(x, y), v(x, y)) = F_{img}(x, y), i(x, y) > 0 \quad (1)$$

$$x = 0, 1, \dots, (H' - 1), y = 0, 1, \dots, (W' - 1)$$

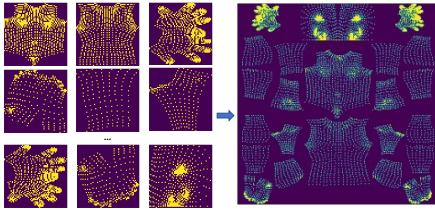


Figure 3: **Illustration of UV map rearrangement.** The original DensePose UV map(left) is part-based. But the density of mapped features varies dramatically. We rearrange the map together according to their actual size and relative position.

This procedure involves rearranging image features in a

structured manner by clustering features belonging to each body part. As shown in Figure 3, the initial UV maps produced by DensePose are part-wise. But the part UV maps are imbalanced compared to a holistic UV map. The actual scale of different body parts varies, leading to a significant difference in the density of valid feature vectors across different maps. And the separation of different parts makes inter-part feature completion challenging. So we map the part-wise UV map into a single map, considering the relative size and position of different parts. We think this arrangement could preserve more neighboring body-part relationships.

3.3. Wrapped Feature Completion

The wrapped feature completion module aims to utilize the visible features to reason the occluded features. The module first uses convolution blocks to downsample the wrapped feature map, and combine the neighboring features. This process enables the module to fuse the features within a body part and those around neighboring parts. To enable the module to consider features across the map, we propose an attention method to further refer to features from different body parts. It applies two 1×1 convolution layers to the downscaled feature map F_{UV}^d to derive body part attention weight \mathcal{A} and attention value \mathcal{V} . Then, it weighted sums the attention value through element-wise matrix mul-

tiplication formulated as:

$$\varphi_i = \sum_{h,w} \sigma(\mathcal{A}) \circ \mathcal{V} \quad (2)$$

where i denotes i^{th} body-part, \circ denotes element-wise multiplication and σ is softmax function that normalizes attention map. As a consequence of feature wrapping, the part feature of different instances is expected to be situated in the same location. Consequently, the attention map for a given part should emphasize a fixed position as the primary reference for the part feature φ_i . Additionally, since various instances may exhibit diverse occlusions, the attention map should also have several other focus areas to obtain information from other parts. It is noteworthy that we train this model without explicit supervision, as the location of the part features is expected to be similar.

3.4. UV Based Feature Inpainting

Using feature wrapping and feature completion module, we have obtained an accurate part-wise feature vector. Our goal is to ensure that these features are robust and invariant to occlusions. Previous methods [27] have relied on data augmentation strategies, such as random cropping or synthetic occlusion, to achieve this goal. However, experiments conducted by Pang *et al.* [42] indicate that such augmentation methods may not be as helpful as previously believed. We recognize that it is challenging for the network to learn similar features when the image is under occlusion. With only SMPL parameter supervision, the model can hardly learn to output similar human features when the image is occluded.

To address this issue, we propose a feature inpainting training method that provides part-wise supervision for occlusion augmentation. As shown in Figure 2, this training method takes two inputs, the original image I and the occluded image I^{occ} augmented by synthetic occlusion. We also add occlusion as a binary mask on the predicted IUUV image, denoted as M_{iuv} and M_{iuv}^{occ} . The network processes both pairs of inputs. The unoccluded part feature vector φ serves as the supervision to regulate the occluded vector φ^{oc} . The objective is to predict similar part features even under occlusion. We model this as a similarity loss formulated as:

$$L_{sim} = \frac{1}{p} \sum_{i=0}^{p-1} \frac{\varphi_i^{oc} \varphi_i}{|\varphi_i^{oc}| |\varphi_i|} \quad (3)$$

This training strategy introduces the ground truth feature to the network, helping the model to inpaint the missing feature.

The inpainted part feature φ_i is flattened and concatenated with global feature average pooled from F_{img} , initial SMPL and camera parameters $(\theta, \beta, \pi)_{init}$. The final fully-connected layer regresses the final parameters (θ, β, π) in an iterative regression manner.

3.5. Loss Functions

We supervise our training with SMPL parameters loss L_{SMPL} , 3D keypoints loss L_{3D} , 2D keypoints L_{2D} and similarity loss L_{sim} that can be formulated as:

$$L = \lambda_{SMPL} L_{SMPL} + \lambda_{3D} L_{3D} + \lambda_{2D} L_{2D} + \lambda_{sim} L_{sim} \quad (4)$$

$$\begin{aligned} L_{SMPL} &= \|(\theta, \beta) - (\hat{\theta}, \hat{\beta})\|, \\ L_{3D} &= \|J_{3D} - \hat{J}_{3D}\|, \\ L_{2D} &= \|J_{2D} - \hat{J}_{2D}\|, \end{aligned} \quad (5)$$

3.6. Implementation Details

We utilize HRNet [4] as the image encoder. Compared to ResNet[17], HRNet’s design preserves more image-aligned features and has a larger resolution feature map output, which makes the wrapped feature more precise and corresponds to the image pixel. We set

We implement DIMR with PyTorch [43] and MMHuman3D [9]. We train DIMR with batch size 128, using Adam [25] optimizer with a learning rate of $2.5e^{-4}$ and batch size 128, we set $\lambda_{SMPL} = 1$, $\lambda_{3D} = 5$, $\lambda_{2D} = 5$, and $\lambda_{sim} = 1$. We take the HRNet-W32 pretrained on COCO poses estimation [36] as the backbone. We first train our model without parallel inpainting for 50K iterations, with random scale, rotation, flipping, and channel noise augmentation. Then we finetune the model in parallel training for 15K iterations with synthetic occlusion.

4. Experiments

Datasets: We train DIMR on model using the standard training sets of Human3.6M[20], COCO[36], and MuCo[39]. We use the ground truth SMPL parameters of Human3.6M and MuCo, and the pseudo ground truth SMPL parameters provided by EFT[22] for COCO. Our evaluation includes multiple human pose datasets. To assess the general performance of the model, we have evaluated it on 3DPW [48]. Moreover, we have evaluated the occlusion handling capability of our model on various subsets of 3DPW, namely 3DPW-OCC, which predominantly contains object occlusion, 3DPW-PC, a person occlusion subset of 3DPW, and 3DOH, an object occlusion dataset. For qualitative assessment, we have employed OCHuman[56], a person occlusion dataset.

IUV Generation. We separately train and test our model on two different sets of IUV images. First we use DensePose [16] to generate the segmentation and predicted IUV images. To assess our model’s full capabilities, we use SMPL parameters to render ground-truth IUV images. Noted that we mask out the invisible portion with a segmentation map, which means the invisible parts won’t have any valid dense

correspondence. The second model is denoted as DIMR (GT IUV).

Evaluation metrics. Our evaluation metrics on the 3D datasets include mean per joint position error (MPJPE), Procrustes-aligned MPJPE (PA-MPJPE), and per-vertex error (PVE) in *mm*. MPJPE and PA-MPJPE assess the accuracy of 3D joint rotation, and PVE evaluates the 3D surface error.

4.1. Comparison to the state-of-the-art

Occlusion Evaluation: Table 1 compares DIMR’s robustness against occlusion with other SOTA occlusion handling methods. We compare our models on occlusion datasets. On 3DPW-PC datasets, our model achieves state-of-the-art performance on 3DPW-OCC dataset. And it has comparable results on other occlusion datasets. On the 3DPW-PC dataset, our model exhibits better performance than OCHMR, a heatmap-based method designed for inter-person occlusion, with a higher PA-MPJPE score. This suggests that our feature extraction method is more accurate compared to the center heatmap-based method, indicating that in terms of accurate pose prediction, our dense map-based method performs better. And comparing to another dense correspondence method PyMAF[54], our model is clearly better, as a dedicated network for map prediction is more robust under human occlusion. On the 3DOH dataset, our model demonstrates comparable performance with the state-of-the-art method PARE[27]. The ground truth model achieves a substantial increase in accuracy, as evidenced by a 50% lower MPJPE on the 3DPW-OCC dataset compared to PARE. On the PA-MPJPE of 3DPW-PC, our model increases performance by 20%. This dramatic increase in performance on person-occlusion subsets demonstrates that with an accurate dense correspondence map, our network can accurately separate visible human features from occluded people.

General Comparison: We compare our model on 3DPW, which is a general dataset. Our results indicate that DIMR, achieves comparable performance when compared to state-of-the-art methods. Furthermore, we observe that our model outperforms occlusion-specific methods such as OCHMR and ROMP, with a lower error rate. We attribute this success to our model’s ability to incorporate both global and local information through our designed architectures, which contribute to the high baseline performance of our model.

Qualitative Comparison: Figure 4 visualizes the qualitative results compared with CLIFF[33] and PARE[27]. We visualize our result on OCHUman[56], 3DPW[48] and 3DOH[57] datasets. DIMR predicts accurate human limbs under object occlusions. Under hard cases like heavy human occlusion, our model is able to predict the correct human with the corresponding limbs, due to the accurate fea-

ture separation based on the dense map.

4.2. Ablation Study

We conduct our ablation study on 3DPW and 3DPW-OC. In the ablation study, we mainly utilize the ground truth IUV setting for comparison.

Effect of UV feature wrapping: We first explore the effect of our feature wrapping technique by modifying the input to our feature completion module. The IUV image provides the network with strong prior knowledge, including dense human information. And the wrapping process provides the network with a piece of structured feature information. To assess the individual value of these features, we design three alternative methods that remove one of these features. For the Table 3, we substituted wrapped feature F_{UV} with the wrapped input image I_{UV} , by wrapping I with M_{IUV} . This setting mainly removes the features of the UV map. For the Table 3-(b) setting, we remove the inverse-wrapped feature and instead concatenate the M_{IUV} with the image feature map F_{img} . We perform feature completion on the original feature map. This setting removes the structured UV map representation but preserves the image feature and dense correspondence. And in the Table 3-(c) setting, we replace the UV map with a randomly organized UV map, which contains less structured neighboring information. The input feature of these three settings is illustrated in Figure 6. Comparing to the original DIMR, setting (a) cause the most decrease in performance, proving the model require local information for accurate regression. Setting (b) shows limited performance even if it utilizes the ground truth IUV image. At last, setting (c) brings a considerable increase in performance compared to (b), indicating the effectiveness of UV wrapping. But still, the neighboring UV brings more feature fusion.

Effect of wrapped feature completion: We further perform analysis on the design of our feature completion module. We compare our proposed design with two other settings. In the first setting, we remove the attention layer and only use the down-sampled F_{UV}^d for the regression, thereby eliminating long-range feature connection. We further replace the convolution down-sample layer with an average-pooling layer, which removes the feature extraction within the body part. Table 4 shows our results of different settings. The setting combined convolution layer and attention layer achieves the best results, suggesting that both the local and long-range feature fusion are critical for optimal performance. We also visualize six different part attention layers, each with four instances, shown in Figure 5. Our attention mechanism effectively attended to similar areas across instances for a given body part, which is desirable since the part feature’s location remains fixed on the wrapped feature map. Furthermore, it attended to different areas depending on the instance, indicating that it is adap-

Methods	3DPW-PC			3DPW-OC			3DOH	
	PA-MPJPE↓	MPJPE↓	PVE↓	PA-MPJPE↓	MPJPE↓	PVE↓	PA-MPJPE↓	MPJPE↓
HMR-EFT [23]	-	-	-	60.9	94.9	111.3	66.2	101.9
SPIN [29]	82.6	129.6	157.6	60.8	95.6	121.6	68.3	104.3
PyMAF [54]	81.3	126.7	154.3	-	-	-	-	-
ROMP [46]	79.7	119.7	152.8	65.9	-	-	-	-
PARE [27]	-	-	-	56.6	90.5	107.9	57.1	88.6
OCHMR [24]	77.1	117.5	149.6	-	-	-	-	-
DIMR (Ours)	70.7	109.2	154.6	56.6	88.6	108.7	58.8	91.7
DIMR (GT IUUV)	54.6	88.9	104.3	50.6	75.2	94.9	50.9	79.3

Table 1: **Evaluation on occlusion datasets 3DPW-PC[24, 48], 3DPW-OC[27, 48] and 3DOH[57].** For a fair comparison, we train our models without 3DPW datasets when evaluate on both of the 3DPW subset. And we train our models without 3DOH train set when evaluating on 3DOH test set.

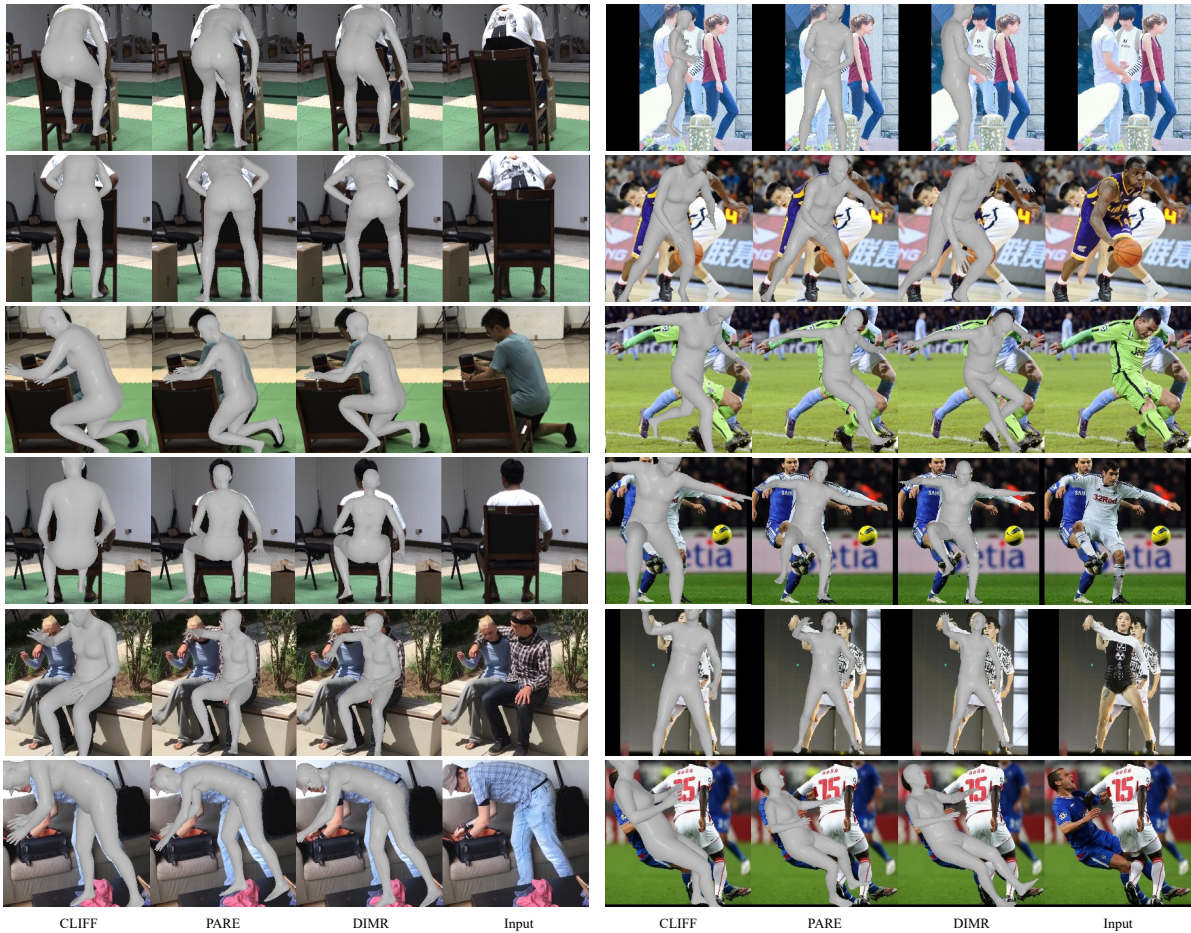


Figure 4: **Qualitative results on 3DOH (left column 1-4), 3DPW (left column 5-6), and OCHuman (right columns) datasets.** DIMR demonstrates higher accuracy in detecting limbs under various types of occlusion. In instances where human subjects heavily overlap, our model can effectively predict the correct limbs with the assistance of a dense correspondence map.

tive. Our attention map also focused on other areas to com-

plete the feature, demonstrating the effectiveness of our at-

Methods		3DPW		
		PA-MPJPE↓	MPJPE↓	PVE↓
General	DecoMR [53]	61.7	-	-
	SPIN [29]	59.2	96.9	116.4
	PyMAF [45]	58.9	92.8	110.1
	HMR-EFT [22]	52.2	85.1	98.7
	METRO [34]	47.9	77.1	88.2
Occlusion	OCHMR [24]	58.3	89.7	107.1
	Pose2UV [18]	57.1	-	-
	ROMP [46]	53.3	85.5	103.1
	PARE [27]	50.9	82	97.9
	DIMR (Ours)	52.9	87	106.6
	DIMR (GT IUUV)	47.8	73.0	99.5

Table 2: **Quantitative comparison results** with state-of-the-art methods on 3DPW. We compare the performance of our method with competing for general methods and occlusion-aware methods.

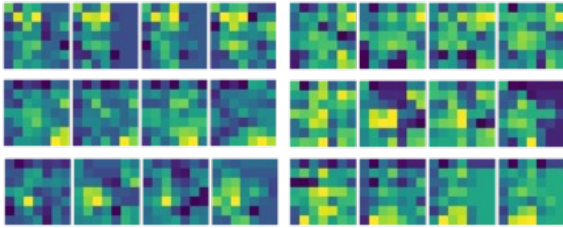


Figure 5: **Attention map visualization:** we visualize 6 different part-attention layers (left 3 columns and right 3 columns), each representing attention for a human part. We show 4 samples for each part. It shows that our attention focus on relatively the same area (yellow colored) across the instances.

Settings	3DPW		
	MPJPE↓	PA-MPJPE↓	PVE↓
w/o UV feature	103.4	59.2	129.5
w/o UV structure	80.8	51.4	106.1
w/o neighboring UV	75.0	49.6	103.1
DIMR	73.0	47.8	99.5

Table 3: **Ablation study on different input feature choices.** We compare three settings that remove one of our design elements: feature wrapping, UV structure, and neighboring UV mapping.

tention design.

Effect of wrapped feature inpainting: In this experiment, we compare our model’s ability to handle occlusion in

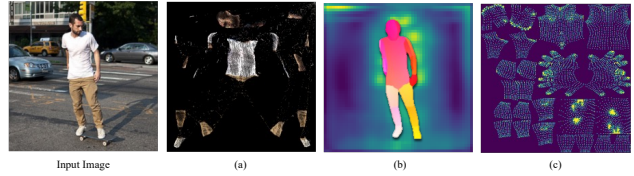


Figure 6: **The illustration of our modified inputs for the ablation study.** (a) replaces the wrapped feature F_{UV} with the wrapped input image I_{UV} ; (b) removes inverse-wrapped feature and instead concatenate the M_{IUUV} with the image feature map F_{img} ; (c) replaces the UV map with a randomly organized UV map.

Settings	3DPW		
	MPJPE↓	PA-MPJPE↓	PVE↓
DIMR	73.0	47.8	99.5
DIMR w/o atten.	79.6	51.1	107.6
DIMR w/o atten. conv.	87.3	53.3	110.8

Table 4: **Ablation study on the input feature.** We compare our original setting with the model without attention and the model without attention and convolution.

Dataset	Settings	PA-MPJPE↓	MPJPE↓
3DPW-OC	synthetic + inpaint	53.4	82.3
	synthetic	53.4	84.2
3DPW	synthetic + inpaint	50.4	79.7
	synthetic	49.0	81.7

Table 5: **Ablation study on inpainting training** We compare the models performance with synthetic occlusion and inpaint training on 3DPW, 3DPW-OC.

the different training settings. We compare models trained with inpainting training and synthetic occlusion with models with only synthetic occlusion. As shown in Table 5, the model utilizing inpainting bring has better accuracy, proving that intermediate supervision is crucial for synthetic occlusion augmentation.

5. Conclusion

We present DIMR, a novel human mesh recovery method robust to object and human occlusions. DIMR draws inspiration from the existing methods tackling occlusion. It combines two fundamental ideas: separating the human feature from occlusion and completing features from invisible cues. We leverage the accurate IUUV map to isolate the part features of the target individual from those of other

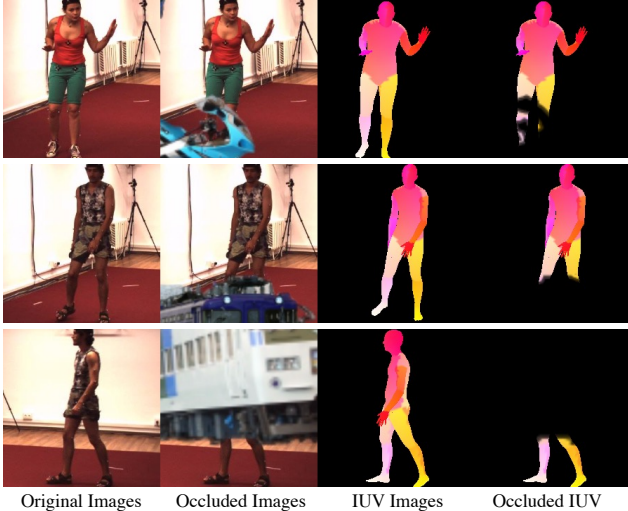


Figure 7: **Illustration of synthetic occlusion.** We place the objects randomly around the center of the image and randomly resize the objects. The IUV image will also be occluded by the objects.

humans. The attention-based feature completion module is then utilized to effectively recover the occluded features using cues from other visible parts. In addition, we adopt an inpainting training strategy to enhance performance in comparison to simple synthetic occlusion. Quantitative and qualitative results prove that our model achieves state-of-the-art performance among occlusion-handling methods and has comparable results on general datasets. Future works can focus on the design of occlusion-robust IUV prediction modules for more accurate human mesh recovery under occlusion.

A. More details on Synthetic Occlusion

We implement the synthetic occlusion following the implementation of PARE [27]. We place objects in Pascal VOC [13] dataset in a random location around the image center and at a random size. We derive the segmentation mask based on the object and mask out the IUV image with the mask. Figure 7 illustrates the occluded IUV image, the image and the original image. It creates various occlusions to the in-door datasets and increase the diversity of simple datasets like Human3.6M [20].

B. Failure Cases

We present visualizations of inaccurate results on OCHuman [56] datasets, as demonstrated in Figure 8. The model is currently unable to effectively handle extreme overlapping, such as a hug, where the similarity between limbs and occlusion of the torso presents challenges to ac-



Figure 8: **Illustration of failure cases.** Top row: failure cases under severe human overlapping. Middle row: failure cases under extreme poses. Bottom row: failure cases under confusing clothes

curate prediction. Additionally, limitations in the training data have resulted in restricted performance when dealing with extreme poses, such as laying down or dance poses. Finally, the presence of dark or dress-like clothing can also contribute to inaccurate predictions. These results highlight the need for further research and development to address these challenges.

C. More Details on IUV Generation

We employ two different methods to generate the IUV images. Firstly, we use the DensePose [16, 49] to predict IUV for all instances in our training and evaluation datasets. For datasets containing single-human instances such as Human3.6M [20], we directly visualize the predictions of the whole image to generate the IUV image. However, for datasets with multiple human instances, such as MuCo [38] and COCO [36], we select the instances based on the intersection over union (IoU) between the predicted and ground truth bounding boxes. We then visualize the predicted IUV image.

We render the IUV images from the ground-truth SMPL model in the second method. For datasets that provide segmentation maps like COCO [36], OCHuman [56], and 3DOH [57], we overlay the instance segmentation mask. And for other datasets [48], we use Mask-RCNN [1] to generate instance masks.

In Figure 9, we present the ground truth IUV image, the rendered IUV image, and the predicted IUV image for comparison. The predicted IUV image preserves occlusion information better than the rendered IUV image. The quality

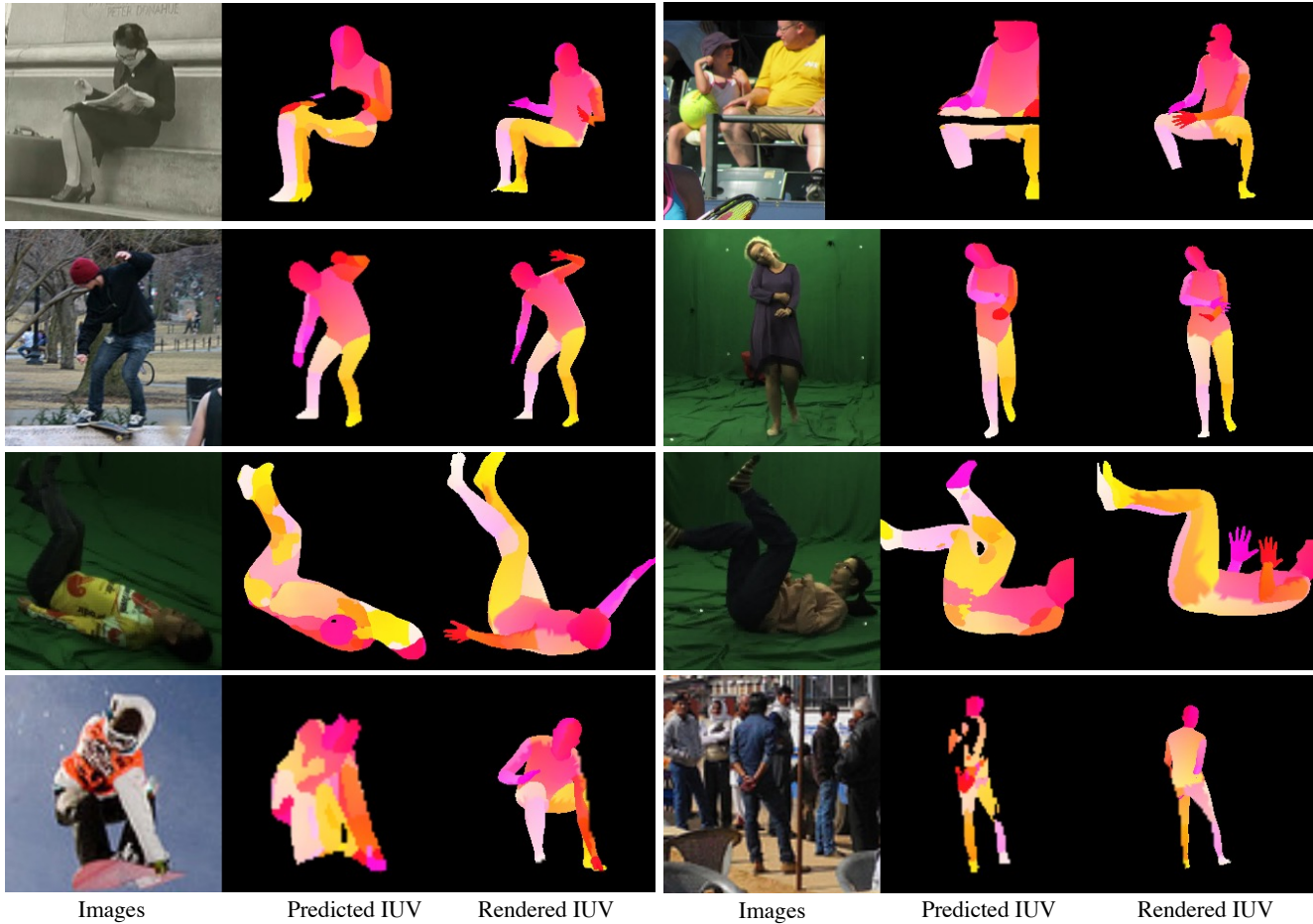


Figure 9: **IUUV images comparison.** Top row shows the predicted IUUV images preserve occlusion and body shape information better. The second row shows accurate predictions when the body is high resolution. The third row shows inaccurate predictions under extreme poses. And the bottom row shows how the image is

of the predicted IUUV image is found to be comparable to the rendered image when the human instance is clear. Furthermore, the predicted IUUV image is more accurate in terms of body shape. However, the quality of prediction is found to be less desirable under extreme poses or when the image is blurred. Since the IUUV prediction model is trained only on COCO [36] dataset, it might be less accurate on out-of-domain data.

References

- [1] Waleed Abdulla. Mask r-cnn for object detection and instance segmentation on keras and tensorflow. https://github.com/matterport/Mask_RCNN, 2017. 9
- [2] Thiemo Alldieck, Gerard Pons-Moll, Christian Theobalt, and Marcus Magnor. Tex2shape: Detailed full human body geometry from a single image. In *IEEE International Conference on Computer Vision (ICCV)*, 2019. 3
- [3] Federica Bogo, Angjoo Kanazawa, Christoph Lassner, Peter Gehler, Javier Romero, and Michael J Black. Keep it smpl: Automatic estimation of 3d human pose and shape from a single image. In *Eur. Conf. Comput. Vis.*, pages 561–578. Springer, 2016. 2
- [4] Bowen Cheng, Bin Xiao, Jingdong Wang, Honghui Shi, Thomas S Huang, and Lei Zhang. Higherhrnet: Scale-aware representation learning for bottom-up human pose estimation. In *Proceedings of the IEEE/CVF conference on computer vision and pattern recognition*, pages 5386–5395, 2020. 5
- [5] Junhyeong Cho, Kim Youwang, and Tae-Hyun Oh. Cross-attention of disentangled modalities for 3d human mesh recovery with transformers. In *Eur. Conf. Comput. Vis.*, pages 342–359. Springer, 2022. 3
- [6] Hongsuk Choi, Gyeongsik Moon, and Kyoung Mu Lee. Pose2mesh: Graph convolutional network for 3d human pose and mesh recovery from a 2d human pose. In *Computer Vision—ECCV 2020: 16th European Conference, Glasgow*,

- UK, August 23–28, 2020, *Proceedings, Part VII 16*, pages 769–787. Springer, 2020. 3
- [7] Hongsuk Choi, Gyeongsik Moon, JoonKyu Park, and Kyoung Mu Lee. Learning to estimate robust 3d human mesh from in-the-wild crowded scenes. In *Proceedings of the IEEE/CVF Conference on Computer Vision and Pattern Recognition (CVPR)*, pages 1475–1484, June 2022. 2, 3
- [8] Vasileios Choutas, Lea Müller, Chun-Hao P. Huang, Siyu Tang, Dimitrios Tzionas, and Michael J. Black. Accurate 3d body shape regression using metric and semantic attributes. In *IEEE Conf. Comput. Vis. Pattern Recog.*, 2022. 2
- [9] MMHuman3D Contributors. Openmmlab 3d human parametric model toolbox and benchmark. <https://github.com/open-mmlab/mmhuman3d>, 2021. 5
- [10] Zhiyang Dou, Cheng Lin, Rui Xu, Lei Yang, Shiqing Xin, Taku Komura, and Wenping Wang. Coverage axis: Inner point selection for 3d shape skeletonization. In *Computer Graphics Forum*, volume 41, pages 419–432. Wiley Online Library, 2022. 3
- [11] Zhiyang Dou, Qingxuan Wu, Cheng Lin, Zeyu Cao, Qiangqiang Wu, Weilin Wan, Taku Komura, and Wenping Wang. Tore: Token reduction for efficient human mesh recovery with transformer. *arXiv preprint arXiv:2211.10705*, 2022. 3
- [12] Zhiyang Dou, Shiqing Xin, Rui Xu, Jian Xu, Yuanfeng Zhou, Shuangmin Chen, Wenping Wang, Xiuyang Zhao, and Changhe Tu. Top-down shape abstraction based on greedy pole selection. *IEEE Transactions on Visualization and Computer Graphics*, 27(10):3982–3993, 2020. 3
- [13] Mark Everingham, Luc Van Gool, Christopher KI Williams, John Winn, and Andrew Zisserman. The pascal visual object classes (voc) challenge. *International journal of computer vision*, 88:303–308, 2009. 9
- [14] Qi Fang, Qing Shuai, Junting Dong, Hujun Bao, and Xiaowei Zhou. Reconstructing 3d human pose by watching humans in the mirror. In *IEEE Conf. Comput. Vis. Pattern Recog.*, 2021. 2
- [15] Peng Guan, Alexander Weiss, Alexandru O Balan, and Michael J Black. Estimating human shape and pose from a single image. In *2009 IEEE 12th International Conference on Computer Vision*, pages 1381–1388. IEEE, 2009. 2
- [16] Rıza Alp Güler, Natalia Neverova, and Iasonas Kokkinos. Densepose: Dense human pose estimation in the wild. In *Proceedings of the IEEE conference on computer vision and pattern recognition*, pages 7297–7306, 2018. 3, 5, 9
- [17] Kaiming He, Xiangyu Zhang, Shaoqing Ren, and Jian Sun. Deep residual learning for image recognition. In *IEEE Conf. Comput. Vis. Pattern Recog.*, pages 770–778, 2016. 5
- [18] Buzhen Huang, Tianshu Zhang, and Yangang Wang. Pose2uv: Single-shot multiperson mesh recovery with deep uv prior. *IEEE Transactions on Image Processing*, 31:4679–4692, 2022. 2, 8
- [19] Yinghao Huang, Federica Bogo, Christoph Lassner, Angjoo Kanazawa, Peter V. Gehler, Javier Romero, Ijaz Akhter, and Michael J. Black. Towards accurate marker-less human shape and pose estimation over time. In *International Conference on 3D Vision (3DV)*, 2017. 2
- [20] Catalin Ionescu, Dragos Papava, Vlad Olaru, and Cristian Sminchisescu. Human3.6m: Large scale datasets and predictive methods for 3d human sensing in natural environments. *IEEE Trans. Pattern Anal. Mach. Intell.*, 36(7):1325–1339, 2013. 5, 9
- [21] Wen Jiang, Nikos Kolotouros, Georgios Pavlakos, Xiaowei Zhou, and Kostas Daniilidis. Coherent reconstruction of multiple humans from a single image. In *CVPR*, 2020. 3
- [22] Hanbyul Joo, Natalia Neverova, and Andrea Vedaldi. Exemplar fine-tuning for 3d human model fitting towards in-the-wild 3d human pose estimation. In *Int. Conf. 3D. Vis.*, pages 42–52. IEEE, 2021. 5, 8
- [23] Angjoo Kanazawa, Michael J Black, David W Jacobs, and Jitendra Malik. End-to-end recovery of human shape and pose. In *IEEE Conf. Comput. Vis. Pattern Recog.*, pages 7122–7131, 2018. 1, 2, 7
- [24] Rawal Khirodkar, Shashank Tripathi, and Kris Kitani. Occluded human mesh recovery. In *IEEE Conf. Comput. Vis. Pattern Recog.*, pages 1715–1725, 2022. 2, 3, 7, 8
- [25] Diederik P Kingma and Jimmy Ba. Adam: A method for stochastic optimization. In *Proc. Int. Conf. Learn. Represent.*, 2015. 5
- [26] Thomas N Kipf and Max Welling. Semi-supervised classification with graph convolutional networks. *arXiv preprint arXiv:1609.02907*, 2016. 3
- [27] Muhammed Kocabas, Chun-Hao P Huang, Otmar Hilliges, and Michael J Black. Pare: Part attention regressor for 3d human body estimation. In *Int. Conf. Comput. Vis.*, pages 11127–11137, 2021. 1, 2, 3, 5, 6, 7, 8, 9
- [28] Muhammed Kocabas, Chun-Hao P Huang, Joachim Tesch, Lea Müller, Otmar Hilliges, and Michael J Black. Spec: Seeing people in the wild with an estimated camera. In *Int. Conf. Comput. Vis.*, pages 11035–11045, 2021. 2
- [29] Nikos Kolotouros, Georgios Pavlakos, Michael J Black, and Kostas Daniilidis. Learning to reconstruct 3d human pose and shape via model-fitting in the loop. In *Int. Conf. Comput. Vis.*, pages 2252–2261, 2019. 2, 7, 8
- [30] Nikos Kolotouros, Georgios Pavlakos, and Kostas Daniilidis. Convolutional mesh regression for single-image human shape reconstruction. In *Proceedings of the IEEE/CVF Conference on Computer Vision and Pattern Recognition*, pages 4501–4510, 2019. 3
- [31] Christoph Lassner, Javier Romero, Martin Kiefel, Federica Bogo, Michael J. Black, and Peter V. Gehler. Unite the people: Closing the loop between 3d and 2d human representations. In *IEEE Conf. on Computer Vision and Pattern Recognition (CVPR)*, July 2017. 2
- [32] Jiefeng Li, Chao Xu, Zhicun Chen, Siyuan Bian, Lixin Yang, and Cewu Lu. Hybrik: A hybrid analytical-neural inverse kinematics solution for 3d human pose and shape estimation. In *IEEE Conf. Comput. Vis. Pattern Recog.*, pages 3383–3393, 2021. 2
- [33] Zhihao Li, Jianzhuang Liu, Zhensong Zhang, Songcen Xu, and Youliang Yan. Cliff: Carrying location information in full frames into human pose and shape estimation. *arXiv: Comp. Res. Repository*, 2022. 2, 6

- [34] Kevin Lin, Lijuan Wang, and Zicheng Liu. End-to-end human pose and mesh reconstruction with transformers. In *Proceedings of the IEEE/CVF conference on computer vision and pattern recognition*, pages 1954–1963, 2021. 3, 8
- [35] Kevin Lin, Lijuan Wang, and Zicheng Liu. Mesh graphormer. In *Int. Conf. Comput. Vis.*, pages 12939–12948, 2021. 3
- [36] Tsung-Yi Lin, Michael Maire, Serge Belongie, James Hays, Pietro Perona, Deva Ramanan, Piotr Dollár, and C Lawrence Zitnick. Microsoft coco: Common objects in context. In *Eur. Conf. Comput. Vis.*, 2014. 5, 9, 10
- [37] Matthew Loper, Naureen Mahmood, Javier Romero, Gerard Pons-Moll, and Michael J Black. Smpl: A skinned multi-person linear model. *ACM Trans. Graph.*, 34(6):1–16, 2015. 1, 3
- [38] Dushyant Mehta, Oleksandr Sotnychenko, Franziska Mueller, Weipeng Xu, Srinath Sridhar, Gerard Pons-Moll, and Christian Theobalt. Single-shot multi-person 3d pose estimation from monocular rgb. In *3D Vision (3DV), 2018 Sixth International Conference on*. IEEE, sep 2018. 3, 9
- [39] Dushyant Mehta, Oleksandr Sotnychenko, Franziska Mueller, Weipeng Xu, Srinath Sridhar, Gerard Pons-Moll, and Christian Theobalt. Single-shot multi-person 3d pose estimation from monocular rgb. In *Int. Conf. 3D. Vis.*, pages 120–130, 2018. 5
- [40] Gyeongsik Moon and Kyoung Mu Lee. I2l-meshnet: Image-to-lixel prediction network for accurate 3d human pose and mesh estimation from a single rgb image. In *Computer Vision–ECCV 2020: 16th European Conference, Glasgow, UK, August 23–28, 2020, Proceedings, Part VII 16*, pages 752–768. Springer, 2020. 3
- [41] Lea Muller, Ahmed AA Osman, Siyu Tang, Chun-Hao P Huang, and Michael J Black. On self-contact and human pose. In *IEEE Conf. Comput. Vis. Pattern Recog.*, pages 9990–9999, 2021. 2
- [42] Hui En Pang, Zhongang Cai, Lei Yang, Tianwei Zhang, and Ziwei Liu. Benchmarking and analyzing 3d human pose and shape estimation beyond algorithms. In *Thirty-sixth Conference on Neural Information Processing Systems Datasets and Benchmarks Track*, 2022. 5
- [43] Adam Paszke, Sam Gross, Francisco Massa, Adam Lerer, James Bradbury, Gregory Chanan, Trevor Killeen, Zeming Lin, Natalia Gimelshein, Luca Antiga, Alban Desmaison, Andreas Kopf, Edward Yang, Zachary DeVito, Martin Raison, Alykhan Tejani, Sasank Chilamkurthy, Benoit Steiner, Lu Fang, Junjie Bai, and Soumith Chintala. Pytorch: An imperative style, high-performance deep learning library. In *Advances in Neural Information Processing Systems 32*, pages 8024–8035. Curran Associates, Inc., 2019. 5
- [44] Georgios Pavlakos, Vasileios Choutas, Nima Ghorbani, Timo Bolkart, Ahmed AA Osman, Dimitrios Tzionas, and Michael J Black. Expressive body capture: 3d hands, face, and body from a single image. In *IEEE Conf. Comput. Vis. Pattern Recog.*, pages 10975–10985, 2019. 1
- [45] Shunsuke Saito, Zeng Huang, Ryota Natsume, Shigeo Morishima, Angjoo Kanazawa, and Hao Li. Pifu: Pixel-aligned implicit function for high-resolution clothed human digitization. In *Int. Conf. Comput. Vis.*, pages 2304–2314, 2019. 8
- [46] Yu Sun, Qian Bao, Wu Liu, Yili Fu, Michael J. Black, and Tao Mei. Monocular, one-stage, regression of multiple 3d people. In *Proceedings of the IEEE/CVF International Conference on Computer Vision (ICCV)*, pages 11179–11188, October 2021. 2, 3, 7, 8
- [47] Yu Sun, Wu Liu, Qian Bao, Yili Fu, Tao Mei, and Michael J. Black. Putting people in their place: Monocular regression of 3d people in depth. In *Proceedings of the IEEE/CVF Conference on Computer Vision and Pattern Recognition (CVPR)*, pages 13243–13252, June 2022. 2, 3
- [48] Timo von Marcard, Roberto Henschel, Michael Black, Bodo Rosenhahn, and Gerard Pons-Moll. Recovering accurate 3D human pose in the wild using IMUs and a moving camera. In *Eur. Conf. Comput. Vis.*, 2018. 2, 5, 6, 7, 9
- [49] Yuxin Wu, Alexander Kirillov, Francisco Massa, Wan-Yen Lo, and Ross Girshick. Detectron2. <https://github.com/facebookresearch/detectron2>, 2019. 9
- [50] Rui Xu, Zhiyang Dou, Ningna Wang, Shiqing Xin, Shuangmin Chen, Mingyan Jiang, Xiaohu Guo, Wenping Wang, and Changhe Tu. Globally consistent normal orientation for point clouds by regularizing the winding-number field. *arXiv preprint arXiv:2304.11605*, 2023. 3
- [51] Rui Xu, Zixiong Wang, Zhiyang Dou, Chen Zong, Shiqing Xin, Mingyan Jiang, Tao Ju, and Changhe Tu. Rfeps: Reconstructing feature-line equipped polygonal surface. *ACM Transactions on Graphics (TOG)*, 41(6):1–15, 2022. 3
- [52] Chunfeng Yao, Jimei Yang, Duygu Ceylan, Yi Zhou, Yang Zhou, and Ming-Hsuan Yang. Learning visibility for robust dense human body estimation. In *European Conference on Computer Vision*, 2022. 2, 3
- [53] Wang Zeng, Wanli Ouyang, Ping Luo, Wentao Liu, and Xiaogang Wang. 3d human mesh regression with dense correspondence. In *IEEE Conf. Comput. Vis. Pattern Recog.*, pages 7054–7063, 2020. 2, 3, 8
- [54] Hongwen Zhang, Yating Tian, Xinchu Zhou, Wanli Ouyang, Yebin Liu, Limin Wang, and Zhenan Sun. Pymaf: 3d human pose and shape regression with pyramidal mesh alignment feedback loop. In *Int. Conf. Comput. Vis.*, 2021. 2, 6, 7
- [55] Nan Zhang, Li Liu, Zhiyang Dou, Xiyue Liu, Xueze Yang, Doudou Miao, Yong Guo, Silan Gu, Yuguo Li, Hua Qian, et al. Close contact behaviors of university and school students in 10 indoor environments. *Journal of Hazardous Materials*, 458:132069, 2023. 3
- [56] Song-Hai Zhang, Ruilong Li, Xin Dong, Paul Rosin, Zixi Cai, Xi Han, Dingcheng Yang, Haozhi Huang, and Shi-Min Hu. Pose2seg: Detection free human instance segmentation. In *Proceedings of the IEEE/CVF conference on computer vision and pattern recognition*, pages 889–898, 2019. 5, 6, 9
- [57] Tianshu Zhang, Buzhen Huang, and Yangang Wang. Object-occluded human shape and pose estimation from a single color image. In *Proceedings of the IEEE/CVF conference on computer vision and pattern recognition*, pages 7376–7385, 2020. 2, 3, 6, 7, 9